

Picometer Level Modeling of a Shared Vertex Double Corner Cube in the Space Interferometry Mission Kite Testbed

Gary M. Kuan^a and Frank G. Dekens^a

^aJet Propulsion Laboratory, California Institute of Technology, 4800 Oak Grove Drive, Pasadena, California, U.S.A.

ABSTRACT

The Space Interferometry Mission (SIM) is a microarcsecond interferometric space telescope that requires picometer level precision measurements of its truss and interferometer baselines. Single-gauge metrology errors due to non-ideal physical characteristics of corner cubes reduce the angular measurement capability of the science instrument. Specifically, the non-common vertex error (NCVE) of a shared vertex, double corner cube introduces micrometer level single-gauge errors in addition to errors due to dihedral angles and reflection phase shifts. A modified SIM Kite Testbed containing an articulating double corner cube is modeled and the results are compared to the experimental testbed data. The results confirm modeling capability and viability of calibration techniques.

Keywords: picometer metrology, interferometry, optical interferometer, corner cube, SIM, Space Interferometry Mission, calibration, modeling

1. INTRODUCTION

The Jet Propulsion Laboratory's Space Interferometry Mission (SIM) is a micro-arcsecond astrometry platform with a mandate to find possible earth sized planets around nearby stars by measuring the distance to and the motion of these stars to high precision. The instrument is comprised of three interferometers having two telescopes each. The angle of the science interferometer baseline to the target star is measured with respect to distant "fixed" reference stars. The accuracy of this relative measurement is dependent on knowledge of the position of each fiducial in the instrument truss as these fiducials define the various interferometer baselines. The legs of the truss are external to the starlight path within each interferometer, and therefore the measurement of the lengths of these legs are referred to as External Metrology. In contrast, Internal Metrology refers to the measurement of the optical path difference between the lengths of the starlight paths originating from each collector bay.

2. THE KITE TESTBED

The SIM Kite Testbed is a two-dimensional, four fiducial, external metrology truss designed to evaluate the measurement capabilities of the SIM metrology subsystem. The purpose of Kite is to demonstrate the ability of interferometric metrology gauges to accurately monitor the position of each fiducial by measuring the legs of the truss, and to predict the length of a "baseline" leg using the measurements of the other legs.

The Kite Testbed, described in detail elsewhere¹ and shown in Figure 1, is made up of four fiducials in a plane with a gauge placed between each pair for a total of six legs. Two of the four fiducials are single, hollow corner cubes while the other two are shared vertex, double corner cubes (DCC's). One of the DCC fiducials is mounted on a two axis gimbal to simulate the articulating motion of the SIM science interferometer siderostat. The wide angle field-of-regard (FOR) spans ± 3.75 degrees of mechanical rotation about the siderostat gimbal axes, while the narrow-angle FOR spans ± 0.5 degrees.

Further author information: (Send correspondence to G.M.K.)

G.M.K.: E-mail: Gary.M.Kuan@jpl.nasa.gov, Telephone: 1 818 393 0270

F.G.D.: E-mail: Frank.G.Dekens@jpl.nasa.gov, Telephone: 1 818 354 7652

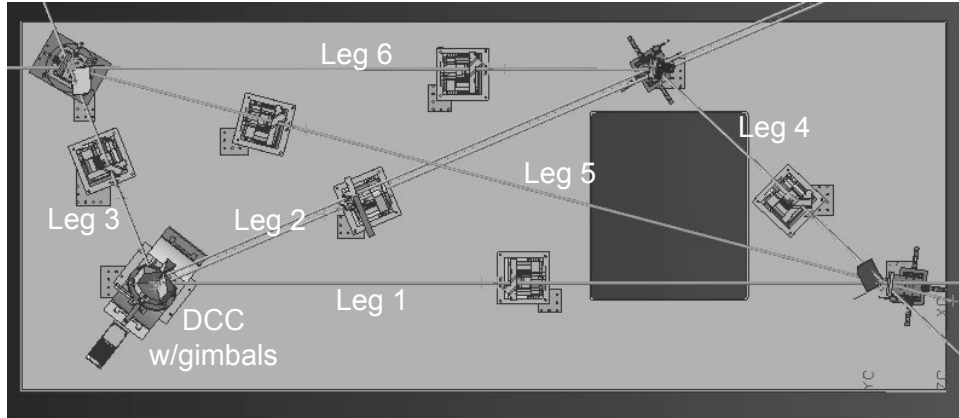


Figure 1. The Kite Testbed Layout: the Kite NCVE configuration includes a shared-vertex, double corner cube (DCC) on gimbals as the articulating fiducial, in contrast to the original layout where the articulating fiducial was a single corner cube. This configuration allows for the effects of non-common vertex error (NCVE) offset to be observed.

The Kite metrology gauges utilize optical interferometry to measure the relative OPD from one observation point in the FOR to another. Only five legs are necessary to find a solution for the truss fiducial positions. The Kite Testbed performance metric is based on the presumption that given measured lengths of any five legs of the truss, the length of the sixth can be predicted. The accuracy of this redundant gauge measurement for the nominal Kite Testbed configuration has previously been reported to be 85pm RMS for wide-angle observations, and a conditional 5.8pm RMS for narrow-angle observations.²

Since then the Kite Testbed has undergone a configuration transformation to include a shared vertex, double corner cube (DCC) as the articulating fiducial instead of a single corner cube. The displacement between the vertices of this DCC is the Non-Common Vertex Error (NCVE) offset. This NCVE contributes an additional geometric truss deformation that is highly field-dependent. The performance of the Kite Model is dependent on the accuracy of our knowledge of the NCVE vector.

2.1. The Double Corner Cube

The shared-vertex, double corner cube (DCC) consists of three 30 degree wedges bonded to a baseplate 90 degrees apart, as shown on the left in Figure 2. Although there are three, hollow, corner cubes available in this design, only two are used in the testbed. This is consistent with the SIM instrument design where DCCs articulate with the Science interferometer siderostat. Triple corner cubes (TCC) of this design are used in the truss to define the shared, Guide interferometer baseline.

The DCC substrate is Zerodur while the reflective coatings are unprotected gold. Geometric manufacturing limitations of primary interest are the dihedral angles and the non-common vertex error (NCVE) offset.

Dihedral angles occur when the corner cube surfaces are not orthogonal. The angular offset between any two reflecting surface from 90 degrees is the dihedral angle. Current DCC dihedral angles are measured to be -0.171, 0.389, and -0.143 arcseconds for CC1 and 0.093, -0.377, and 0.054 arcseconds for CC2.

Figure 2 also shows the NCVE offset vector. Since only two corner cubes are used, there is only one NCVE offset of concern. As a consequence of the DCC design, the NCVE vector resides on the same plane as the baseplate reflecting surface. Although the NCVE is confined to a two-dimensional surface, neither the DCC baseplate nor the NCVE vector are coplanar with the Kite truss plane.

In the testbed layout, the vertex of CC1 is aligned to the gimbal pivot point, while the vertex of CC2 experiences the full effect of the NCVE lever arm as the DCC articulates. Consequently, only the metrology gauge in Leg 3 sees the NCVE vector. This lever arm action introduces six degrees of freedom to the corner cube vertex and surfaces. The aplanarity of the Kite truss as the DCC articulates over the FOR is observed and manifests as a field-dependent change in the length of Leg 3.

Measurement of the NCVE vector was performed at JPL using a testbed designed specifically for this task, though a discourse on this feat is too lengthy to be presented here. The measured NCVE vector of the DCC used in the Kite Testbed was reported to be $[x, y] = [-0.32\mu\text{m} \pm 0.012\mu\text{m}, -3.96\mu\text{m} \pm 0.006\mu\text{m}]$ in a pre-defined local coordinate system where the z-axis is parallel to the unit normal of the baseplate surface.³ The goal of the NCVE Testbed is to measure the NCVE to within $1\mu\text{m}$ of the vector magnitude.

The surface roughness of the reflecting surfaces on the DCC are measured to be less than 6.2nm RMS and 31nm PTV.

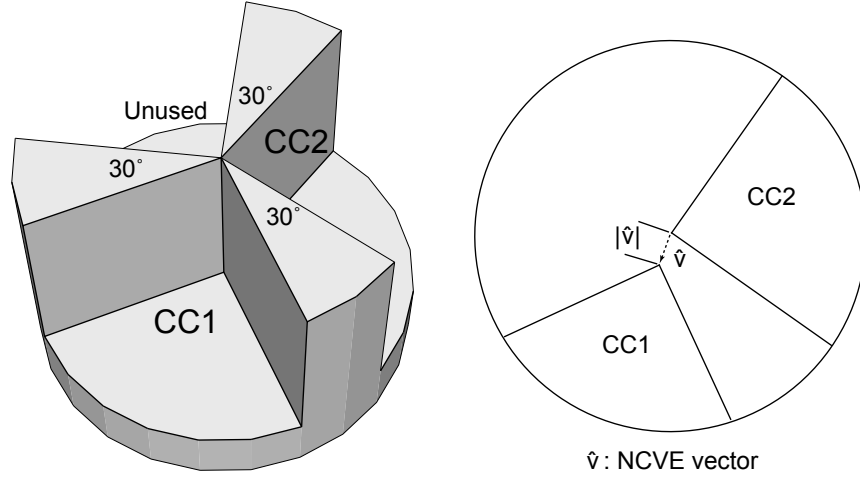


Figure 2. Double Corner Cube: the DCC consists of three 30 degree wedges bonded to a single circular baseplate. Although three corner cubes are available, only two are being used in this testbed.

3. THE KITE MODEL

The Kite Model is based on a single ray raytrace that involves ray electric field propagation and reflection.² In addition to the Testbed geometry and interferometric technique of the metrology gauges, the model reflects three primary physical characteristics of the corner cube fiducials: the corner cube dihedral angle offsets, the index of refraction of the reflective coating, and the Non-Common Vertex Error of the DCC. Although the effect of these characteristics on the OPD of each leg may be small, the nanometer level errors are large when compared to double digit picometers. The performance of the model is highly dependent on the precision and accuracy of our ability to measure these characteristics.

Although SIM external metrology involves two forms of metrology measurements – absolute metrology and relative metrology – we will focus primarily on relative metrology which measures the relative change of the optical path length from one Field-of-Regard (FOR) measurement to another. In other words, relative metrology measures the optical path difference (OPD) over the entire FOR relative to an arbitrary nominal target within the FOR.

The single-gauge OPD is modeled by computing the phase of the metrology beam electric field with respect to the original reference phase after traversing between the two fiducials. The intensity of the interfering electric fields is our measurable quantity. An illustration of a metrology gauge between two fiducials is shown in Figure 3.

The intensity, I , of the interfering measurement and local oscillator electric fields, E_m and E_{lo} , on the detector is

$$I = (E_m + E_{lo})(E_m + E_{lo})^* \quad (1)$$

$$= |E_m|^2 + |E_{lo}|^2 + (E_m E_{lo}^* + E_m^* E_{lo}). \quad (2)$$

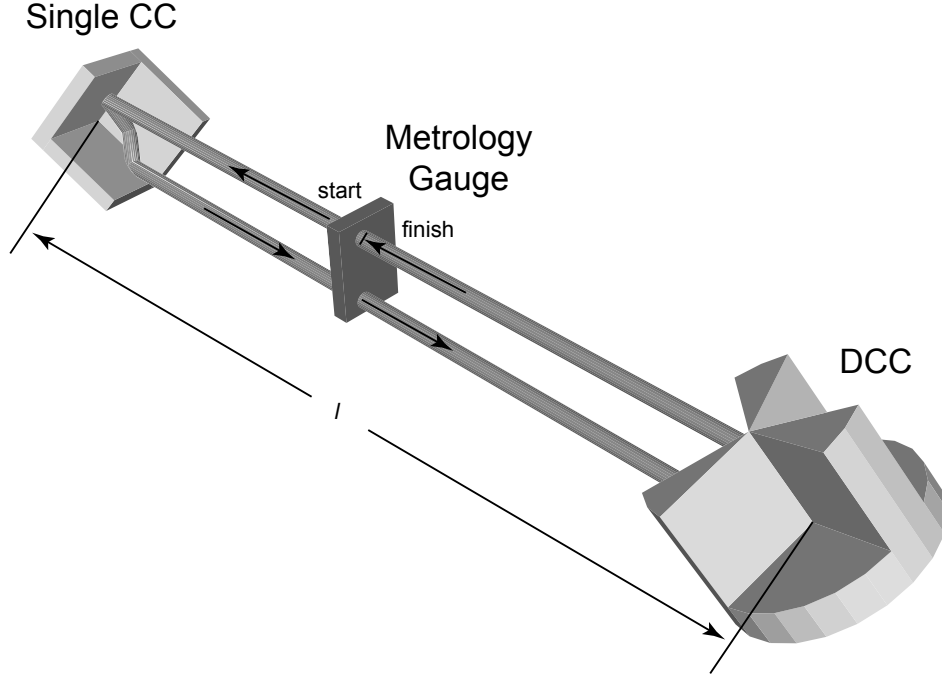


Figure 3. Single gauge between corner cubes. A single metrology gauge measures the distance between corner cube fiducials using optical interferometry. The phase delay experienced by the metrology beam is affected by corner cube dihedral, reflection phase shift, and vertex motion introduced by the NCVE vector.

The last term, in parentheses, is the heterodyne intensity, I_H , that results in the expression below when expanded.

$$I_H = E_m E_{l_o}^* + E_m^* E_{l_o} \quad (3)$$

$$= |E_m| \exp \{+i [\Delta\phi - \phi_o]\} |E_{l_o}| \exp \{+i\phi_o\} + |E_m| \exp \{-i [\Delta\phi - \phi_o]\} |E_{l_o}| \exp \{-i\phi_o\} \quad (4)$$

$$= 2|E_m||E_{l_o}| \cos(\Delta\phi) \quad (5)$$

The phase of the reference beam is ϕ_o and the phase delay of the measurement beam is $\Delta\phi$. Therefore, the phase of the detected heterodyne signal is entirely due to the phase delay as experienced by the measurement beam as it propagates along a racetrack-like path between the two fiducial corner cubes. The OPD, l , at each point of the FOR is computed using the equation

$$l = \frac{1}{2} \frac{\Delta\phi}{2\pi} \lambda \quad (6)$$

where l is the measured distance between the two fiducial vertices and the wavelength, λ , is 1319nm.

3.1. Separation of Free Space Propagation from Reflection Phase Shifts

In order to compute the correct phase delay, the electric field along the metrology optical path must be properly book-kept as the measurement beam propagates from surface to surface.

As the beam propagates, the nominal, linearly polarized, electric field, \vec{E}_o with zero initial phase is subject to a free-space propagation phase delay up to the first reflective surface.

$$\vec{E}^{(i)} = \vec{E}_o \exp \left(+i \frac{2\pi n_o l}{\lambda} \right) \quad (7)$$

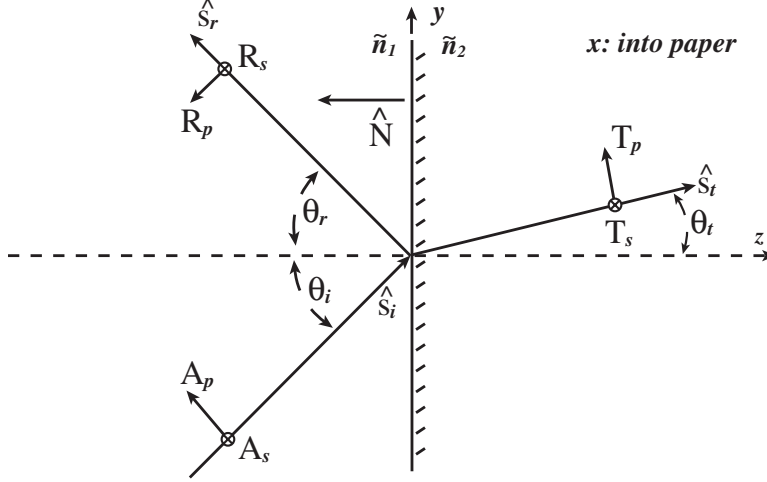


Figure 4. Reflection and Transmission Diagram. This diagram shows the convention used to compute the Fresnel Reflection Coefficients used in the model. Care was taken to keep the index of refraction of the gold reflection surface consistent with the form of the time-invariant electric-field equation.

At the reflecting surface, the incident electric field polarization vector may be expanded into S - and P -polarization components with respect to the unit normal vector of the reflecting surface such that

$$\vec{E}^{(i)} = \left(A_s \hat{s}^{(i)} + A_p \hat{p}^{(i)} \right) \exp \left(+i \frac{2\pi n_o l}{\lambda} \right) \quad (8)$$

where $\vec{E}_o = A_s \hat{s}^{(i)} + A_p \hat{p}^{(i)}$.

As a consequence of the complex index of refraction of the unprotected gold reflective coating, the S - and P - polarizations experience S - and P - Fresnel reflections, respectively (Figure 4).² Therefore, the electric field immediately after reflection becomes,

$$\vec{E}^{(r)} = \left(R_s \hat{s}^{(r)} + R_p \hat{p}^{(r)} \right) \exp \left(+i \frac{2\pi n_o l}{\lambda} \right) \quad (9)$$

$$= \left(A_s \tilde{C}_s^{(r)} \hat{s}^{(r)} + A_p \tilde{C}_p^{(r)} \hat{p}^{(r)} \right) \exp \left(+i \frac{2\pi n_o l}{\lambda} \right), \quad (10)$$

where $\tilde{C}_s^{(r)}$ and $\tilde{C}_p^{(r)}$ are the Fresnel Reflection Coefficients. The Fresnel Reflection Coefficients are generally complex⁴ and can be expressed in terms of attenuation and phase.

$$\tilde{C}_s^{(r)} = \left| \tilde{C}_s^{(r)} \right| \exp(i\phi_s) \quad (11)$$

$$\tilde{C}_p^{(r)} = \left| \tilde{C}_p^{(r)} \right| \exp(i\phi_p). \quad (12)$$

It is important to note that while a beam propagating in free space experiences a phase delay that is common to all polarization states, the same beam reflecting from a gold surface experiences different phase delays for its S - and P - polarization states. Since our measurement beam reflects from six corner cubes surfaces at six different angles of incidence to six different surface normals, it is imperative that the electric field be carefully recomputed after each reflection.

The total phase delay due to free space propagation through m number of segments is

$$\Delta\phi_L = \frac{2\pi n_o L}{\lambda} \quad (13)$$

where $L = l_1 + l_2 + \dots + l_m$ is the total optical path length (OPL) along the propagation direction. This free space propagation is common to both S - and P - polarization states for any and all surfaces and thus is separable from the reflection phase shifts.

The measurement beam electric field, E_m , at the detector plane where the measurement beam and the local oscillator interfere can therefore be expressed in general form as

$$E_m = (|E_{mp}| \vec{p} + |E_{ms}| \vec{s}) \exp\left(+i \frac{2\pi n_o L}{\lambda}\right) \quad (14)$$

Since the measurement beam interferes with a linearly polarized local oscillator, the portion of the electric field in the same polarization state as the local oscillator, E'_m , is

$$E'_m = |E'_m| \exp(+i\phi_r) \exp\left(+i \frac{2\pi n_o L}{\lambda}\right) \quad (15)$$

$$= |E'_m| \exp(+i\phi_r) \exp(+i\phi_L) \quad (16)$$

$$= |E'_m| \exp[+i(\phi_r + \phi_L)] \quad (17)$$

where

$$\phi_L = \frac{2\pi n_o L}{\lambda}. \quad (18)$$

The total phase change at the detector, $\Delta\phi$, is

$$\Delta\phi = \phi_r + \phi_L \quad (19)$$

where ϕ_r is the phase change due to reflection phase shifts, and ϕ_L is the phase change due to free space propagation.

The OPL can therefore be separated into two parts such that

$$l = \frac{1}{2} \frac{\lambda}{2\pi} \Delta\phi \quad (20)$$

$$= \frac{1}{2} \frac{\lambda}{2\pi} (\phi_r + \phi_L) \quad (21)$$

$$= \frac{1}{2} \frac{\lambda}{2\pi} \phi_r + \frac{1}{2} \frac{\lambda}{2\pi} \phi_L \quad (22)$$

$$= l_r + l_L \quad (23)$$

4. RESULTS: TESTBED VS. MODEL

The Kite Testbed wide-angle observing scenario consists of 30 second "looks" separated by 15 second slew and acquisition segments. A single SIM observing tile lasts 1 hour and includes many "looks" spanning a 15 degree cone on the sky. The Kite Testbed simulates this scenario by tilting the DCC over a mechanical ± 3.75 degree cone using the same observation timing scheme. The observation scan over the FOR is designed to remove effects of temporal drift due to thermal and other field-independent sources. The Kite wide-angle scenario is described in more detail elsewhere.¹

The Kite Error Metric is intended to measure the ability of the redundant truss to predict the measurement by any single gauge. For a planar, four node truss with six legs, only knowledge of the lengths of five legs are necessary to find a solution for the node positions and thus the length of the sixth leg. In order to observe the effects of NCVE, we choose to compute the error metric for Leg 3 such that

$$\text{Metric}(\mathbf{u}, \mathbf{v}) = f_{L_3} (L_1(\mathbf{u}, \mathbf{v}), L_2(\mathbf{u}, \mathbf{v}), L_4, L_5, L_6) - L_3(\mathbf{u}, \mathbf{v}), \quad (24)$$

where L_i is the single gauge measurement for leg i , f_{L_3} is the length of L_3 based on measurement of the other five legs, and u and v are siderostat angles on the sky. L_4 , L_5 , and L_6 do not see the DCC and are therefore constant with respect to the field-of-regard. The general form of Equation 24 is also referred to as the “five-minus-one” metric.

The measured length of each individual leg is the sum of the absolute and relative metrology measurements. A single absolute metrology run is conducted prior to a set of wide-angle observing runs, and is assumed valid for the duration.

4.1. Single Gauge Calibration Method

One application of the model is to calibrate each individual metrology gauge measurement prior to applying the five-minus-one function and computing the error metric. This is repeated for every observing point over the field-of-regard, resulting in a two-dimensional data set representing the residual error metric.

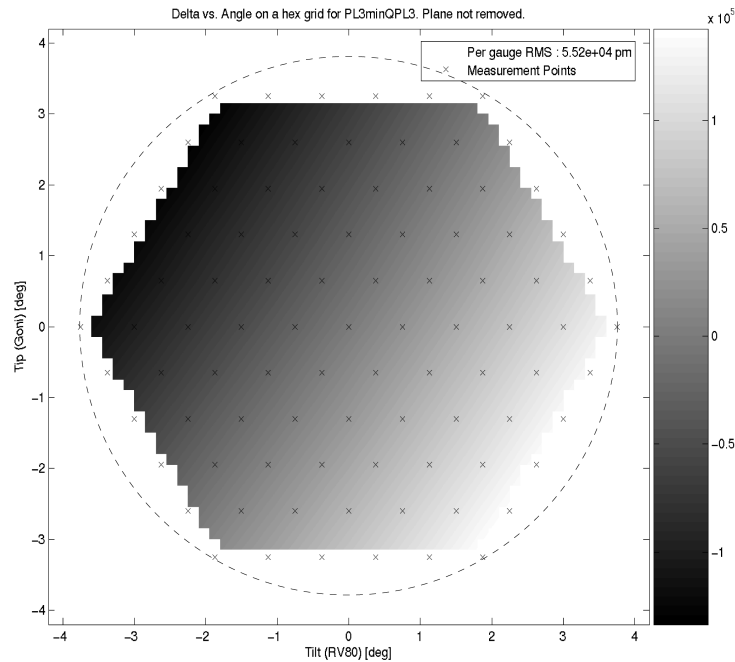


Figure 5. Kite Testbed Wide-Angle Error Metric Data. This is the “five-minus-one” prediction error of the redundant truss over the Field-of-Regard. Each measurement point is a mean of many data runs. A very large linear component is evident and attributed to the newly introduced NCVE offset.

This method of gauge calibration is also a test of model validity. Given the parameters included in the model – such as truss geometry, dihedral, NCVE, refractive index, and absolute metrology measurements – calibration of each individual gauge before performing the Kite Metric analysis provides a way of assessing the performance of the model with respect to actual testbed measurements. If the measurement biases of the calibrated system are significantly reduced, then it is evidence that the model does enable prediction of measurement errors produced by the influence of non-ideal testbed components on interferometric phase measurements. The goal, of course, is to refine the model such that the most influential physics based elements are captured and the residual error is reduced to negligible levels.

In the case of the Kite Testbed, multiple experimental observations over the FOR are taken over many days and weeks. The mean Kite Error Metric is shown in Figure 5. A large first order gradient is apparent – much larger than was seen in the previous Kite configuration.

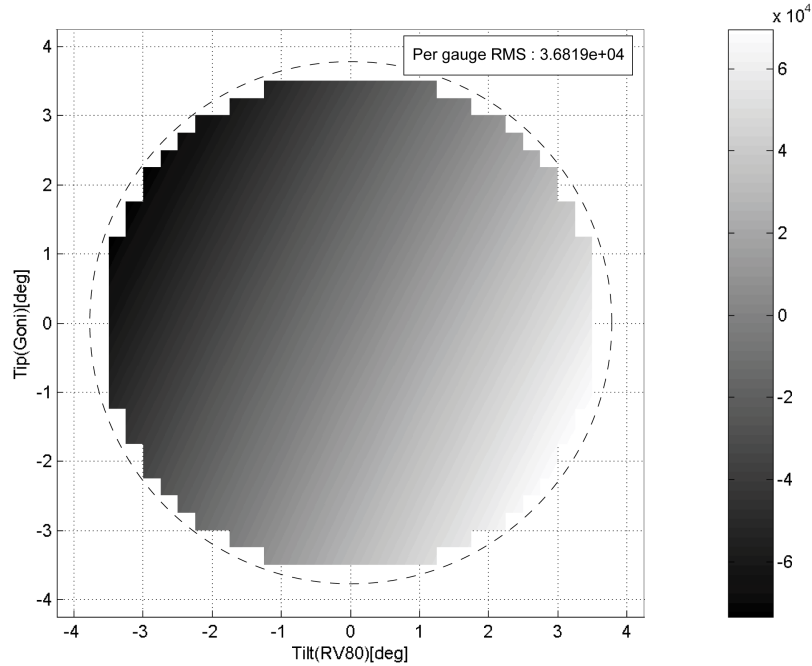


Figure 6. Kite Model Wide-Angle Error Metric Data. This is the "five-minus-one" prediction error of the redundant truss over the Field-of-View. The model includes NCVE offset, dihedral angles, and reflection phase shifts due to the complex refractive index of the unprotected gold coatings.

Since the FOR is represented by two rotation variables – tip (u) and tilt (v) – representing the angle on the sky, the error metric or residual error metric data sets are circular and may be decomposed into Zernike coefficients for analysis. The Zernike coefficients of the raw experimental data are shown in Table 1. Both the mean and standard deviation of the first ten coefficients are listed. The terms having the greatest bias on the Kite metric are tip and tilt, followed by piston and focus.

Also included in the table are the Kite metric Zernike coefficients after each single gauge measurement is calibrated by removing the bias predicted by the model. The resultant Zernikes of the calibrated five-minus-one prediction errors are significantly reduced by greater than 75% for piston, tip, tilt, and focus. Many of the higher order terms are also reduced, though by lower percentages. Ignoring the uniform piston coefficient, the greatest overall reduction occurs in the linear terms of tip and tilt, where 28.5 and 35.7 nanometers RMS of error are removed. This is a 93% and 78% reduction in the redundant truss prediction error bias, respectively, due solely to physical, corner cube parameters. In total, the model-calibrated testbed prediction error has been reduced by 82% from 54.7nm RMS to 9.8nm RMS.

A reverse analysis of the testbed data reveals that, to first order, an NCVE magnitude of $2.35\mu\text{m}$ is necessary to produce the systematic error observed. This same analysis applied to the calibrated testbed data indicates an expected NCVE magnitude of $0.279\mu\text{m}$. This is well within the $\pm 1\mu\text{m}$ measurement accuracy of the NCVE Measurement Testbed.

In relation to the SIM instrument, the model-calibrated testbed data has an even greater significance. SIM will be using reference stars within the field-of-view, or tile, to fit and remove a plane from measurements. As a result, reduction of second order and higher Zernike coefficients are of great interest. The RMS of the non-linear, non-calibrated testbed data is 1077pm, while the RMS of the non-linear, calibrated testbed data is 173pm, a reduction of 84%. Although this residual prediction error is greater than the required 140pm, it is a significant step in the right direction.

Table 1. Kite Wide Angle Data Table. With and without model removed. The total RMS is the RSS of all the Zernike Coefficients. The non-linear RMS is the RSS of coefficients above first order.

Zernike	Raw Data		Model Removed	
	mean [pm]	σ [pm]	mean [pm]	σ [pm]
piston	1930	296	329	299
tip (sin)	-30509	276	-1925	278
tilt (cos)	45337	282	-9593	282
astigmatism (sin)	69	30	65	30
focus	1060	154	137	154
astigmatism (cos)	154	36	56	36
trefoil (sin)	-24	69	-9	70
coma (sin)	-5	76	-10	77
coma (cos)	69	45	53	45
trefoil (cos)	48	48	26	49
Total RMS:	54691		9791	
non-linear RMS:	1077		173	

Furthermore, it is not entirely unexpected that the non-linear residual prediction error is not below the SIM requirement since the surface figure of the brassboard DCC is not as smooth and flat as the single, hollow, Super Corner Cube (SCC) used in the earlier Kite Testbed configuration. This issue has been addressed and will be described in future manuscripts.

5. CONCLUSION

The Space Interferometry Mission is a complex optical space platform that requires both accurate and precise onboard metrology. The External Metrology subsystem involves the monitoring of baseline length and orientation by measuring relative changes in position of the corner cube fiducials. Manufacturing limitations of these corner cubes introduce field-dependent measurement errors that must be calibrated out in order to maintain microarcsecond astrometric performance. The inclusion of a non-common vertex error offset in our Double Corner Cube fiducials requires further enhancement to our Kite testbed model. Single-gauge calibration of the Kite Testbed using the refined model has reduced the overall five-minus-one prediction error from 54.7nm RMS to 9.8nm RMS. In addition, the non-linear error metric has been reduced from 1.077nm RMS down to 173pm RMS.

Refinement of the model is ongoing. Inclusion of surface roughness on all reflective surfaces and mechanical jitter in the pointing mechanism of each metrology gauge as well as the steering gimbals of the DCC will be presented in the future. In the meantime, confidence in the validity of the model has allowed its use as a tool for sensitivity analysis and refinement of requirements on corner cube manufacturing and alignment tolerances.

ACKNOWLEDGMENTS

Many thanks to the entire Kite Testbed team, including Tim Neville, Ian Crossfield, Dan Ryan, Alireza Azizi, John Negron, and Steven Moser. We would also like to thank Bijan Nemati for his tireless work as former Kite Testbed lead and his continuing support of those of us following in his footsteps. The research described in this paper was carried out at the Jet Propulsion Laboratory, California Institute of Technology, under a contract with the National Aeronautics and Space Administration.

REFERENCES

1. F. G. Dekens, O. S. Alvarez-Salazar, A. Azizi, S. J. Moser, B. Nemati, J. Negron, T. Neville, and D. Ryan, "Kite: status of the external metrology testbed for SIM," *New Frontiers in Stellar Interferometry* **5491**(1), pp. 1020–1033, SPIE, 2004.

2. B. Nemati and G. M. Kuan, “Model validation of SIM external metrology at the sub-nanometer level,” *New Frontiers in Stellar Interferometry* **5491**(1), pp. 1823–1834, SPIE, 2004.
3. D. Ryan, A. Azizi, D. Moore, J. Negron, M. Marcin, T. Neville, S. Moser, L. Wayne, I. Crossfield, and P. Best, “The non-common vertex error testbed result document.” internal memo, Jet Propulsion Laboratory, California Institute of Technology, December 2005.
4. M. Born and E. Wolf, *Principles of Optics*, Cambridge University Press, 7th ed., 1999.